Article

Cell Chemical Biology

Structure-based Engineering of a Plant-Fungal Hybrid Peroxidase for Enhanced Temperature and pH Tolerance

Graphical Abstract

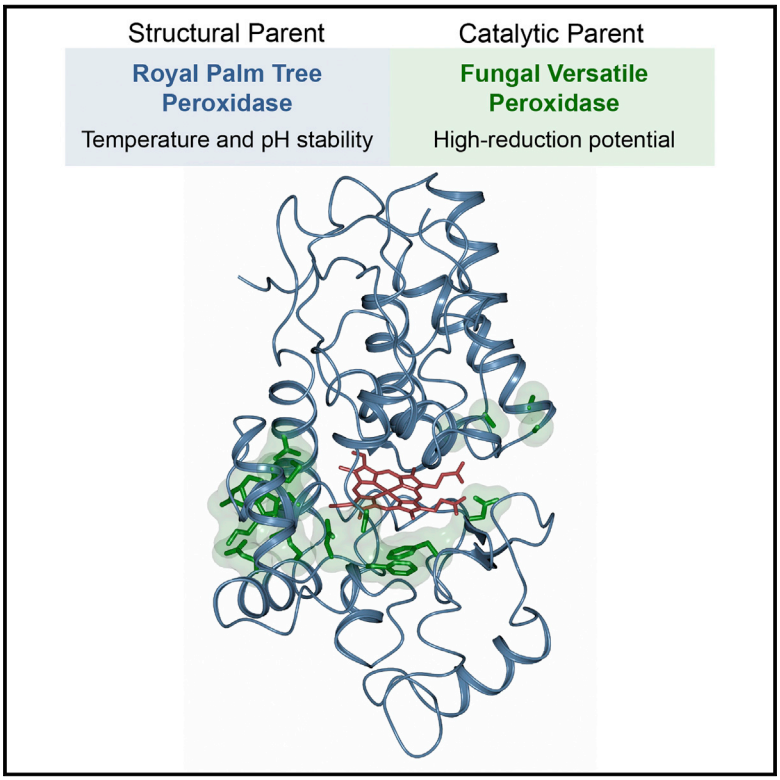

Highlights

- Structure-based engineering enables design of peroxidase with wider utility
- Catalytic versatility of engineered peroxidase (VP2.0) comparable with catalytic parent
- VP2.0 retains activity over broader temperature and pH ranges
- VP2.0 exhibits greater structural stability under optimal reaction conditions

Authors

Amanda C. Kohler, Blake A. Simmons, Kenneth L. Sale

Correspondence

klsale@sandia.gov

In Brief

Kohler et al. describe a rational engineering approach for the direct design of innovative, industrially tailored biocatalysts. They utilize this approach to address the current application barrier of high-reduction potential peroxidases as oxidative tools, building a catalytically versatile plant-fungal hybrid peroxidase capable of functioning under wider temperature and pH ranges.

Kohler et al., 2018, Cell Chemical Biology *25*, 974–983
August 16, 2018
https://doi.org/10.1016/j.chembiol.2018.04.014

CellPress

CellPress

Cell Chemical Biology
Article

Structure-based Engineering of a Plant-Fungal Hybrid Peroxidase for Enhanced Temperature and pH Tolerance

Amanda C. Kohler,[1,2,4] Blake A. Simmons,[1,3] and Kenneth L. Sale[1,2,5,*]
[1]Joint BioEnergy Institute, Emeryville, CA 94608, USA
[2]Biomass Science and Conversion Technology Department, Sandia National Laboratories, Livermore, CA 94550, USA
[3]Biological Systems and Engineering, Lawrence Berkeley National Laboratory, Berkeley, CA 94720, USA
[4]Present address: Plexxikon Inc., Berkeley, CA 94710, USA
[5]Lead Contact
*Correspondence: klsale@sandia.gov
https://doi.org/10.1016/j.chembiol.2018.04.014

SUMMARY

In an age of ever-increasing biotechnological and industrial demand for new and specialized biocatalysts, rational protein engineering offers a direct approach to enzyme design and innovation. Heme peroxidases, as indispensable oxidative biocatalysts, provide a relatively mild alternative to the traditional harsh, and often toxic, chemical catalysts, and subsequently, have found widespread application throughout industry. However, the potential for these enzymes is far greater than their present use, as processes are currently restricted to the more stable, but less catalytically powerful, subset of peroxidases. Here we describe the structure-guided, rational engineering of a plant-fungal hybrid peroxidase built to overcome the application barrier of these high-reduction potential peroxidases. This engineered enzyme has the catalytic versatility and oxidative ability of a high-reduction potential versatile peroxidase, with enhanced temperature and pH tolerance similar to that of a highly stable plant peroxidase.

INTRODUCTION

Heme peroxidases catalyze the one-electron oxidation of organic and inorganic compounds, and their catalytic mechanism is driven by the oxidation-reduction cycle of their heme-iron center (de Montellano, 2010). These enzymes offer a much-needed alternative to harsh chemical catalysts, and, therefore, have gained valuable application in medical diagnostics, biosensor technology, decolorization of synthetic dyes in photography and textile manufacturing, and in fine chemical and polymer synthesis (Ayala and Torres, 2016; Isaac and Dawson, 1999). Their potential, particularly those with higher oxidative power, extends to remediation of emerging pollutants, such as pesticides, pharmaceuticals, and other household chemicals that accumulate in waterways and adversely affect human health (Deblonde et al., 2011; Eibes et al., 2011; Wen et al., 2009). An adequate remediation method for these water pollutants is not currently available, and high-reduction potential peroxidases offer a means of transforming these compounds into less harmful derivatives. Similarly, as society turns to a more bio-based economy, the need to develop conversion technologies aimed at addressing the degradation and valorization of the large quantities of lignin waste generated by industrial biorefineries and pulp and paper mills will likely increase (Busse and Czermak, 2016). High-reduction potential heme peroxidases, as sustainable, environmentally friendly, and catalytically powerful biocatalysts, are likely to be a key component in the solution to these current and future challenges.

Of the high-reduction potential peroxidases, versatile peroxidases (VPs) are of particular industrial interest, because they have the catalytic versatility to directly oxidize a range of low- and high-reduction potential aromatic substrates and indirectly oxidize these substrates through oxidation of manganese, which acts as a diffusible oxidizer (Camarero et al., 1999; Knop et al., 2016; Pérez-Boada et al., 2005). VPs are evolutionarily related to secretory plant and extracellular fungal heme peroxidases, and share significant structural homology with these enzymes (Zamocky et al., 2015). These peroxidases are predominantly α-helical in structure with calcium coordination sites and disulfide bridges to aid in structure stabilization (Ruiz-Duenas et al., 2009; Watanabe et al., 2010). Essential to their catalytic function, VPs contain an internally coordinated heme molecule and oxidation pathways that lead from the enzyme surface to the heme center, facilitating heme access and long-range electron transfer (LRET) (Ruiz-Duenas et al., 2009; Smith and Veitch, 1998). VPs owe their catalytic versatility to the presence of three oxidation pathways: (1) a manganese oxidation site; (2) an exposed heme edge, also found in general peroxidases, that directly oxidizes phenols, amines, and small dye compounds; and (3) an LRET pathway capable of high-reduction potential aromatic oxidation (Knop et al., 2016) (Figures 1A–1C).

Mechanistically, VPs follow one of two catalytic cycles (Figure 1D). The first of these cycles is very similar to that of general peroxidases and enables VP to directly target low-reduction potential substrates and indirectly target high-reduction potential substrates through the oxidation of diffusible manganese

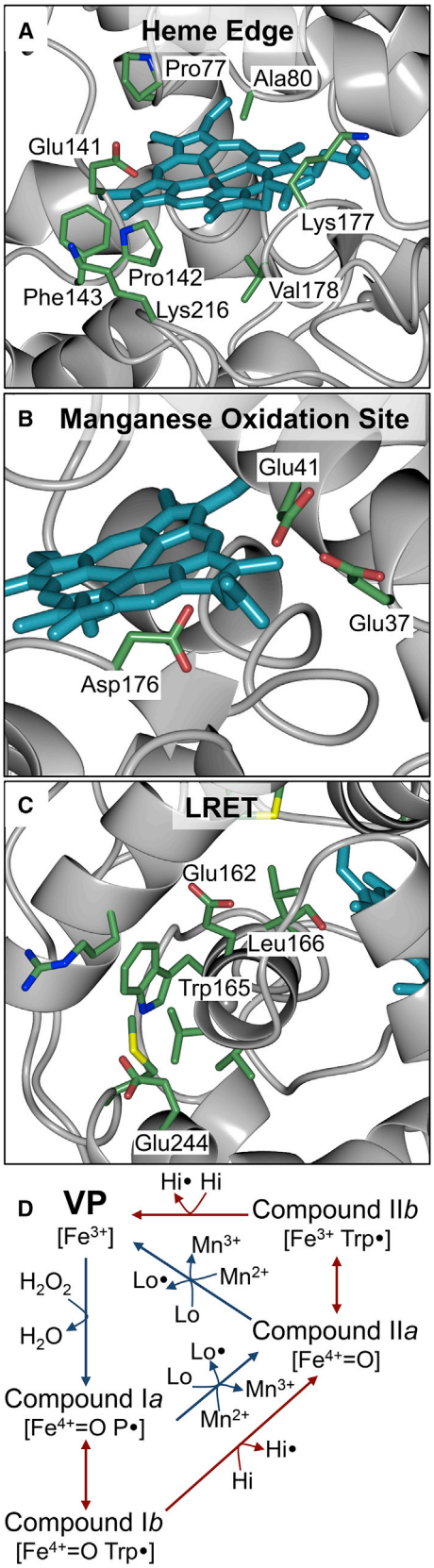

Figure 1. The Oxidation Pathways and Catalytic Cycle of Versatile Peroxidase VP1

(A–C) The structure of VP1 (PDB ID: 4BLL [Fernandez-Fueyo et al., 2014b]) is depicted in gray with the residues involved in each of its three oxidation pathways displayed: (A) heme edge, (B) manganese oxidation site, and (C) LRET. For the LRET pathway, only key functional residues are labeled. Heme is illustrated in cyan.

(D) The catalytic cycle for a versatile peroxidase (VP) proposed by Pérez-Boada et al. (2005) involves formation of Compound I*a*/*Ib* upon a two-electron oxidation of the heme-iron center by hydrogen peroxide. The resting iron (III) state is oxidized to form the iron (IV)-oxo and either the heme porphyrin cation radical (P•) (Compound I*a*) or the tryptophan radical (Trp•) (Compound I*b*). Formation of Compound I*a* activates VP's low-reduction potential oxidation route (denoted with blue arrows). From Compound I*a*, the enzyme can then oxidize manganese or low-reduction potential aromatic substrates (Lo) via its manganese oxidation site or exposed heme edge, respectively, to yield Compound II*a* (iron [IV]-oxo) and can then oxidize a second manganese or low-reduction potential substrate to return to its resting state. Alternatively, upon formation of Compound I*b*, VP can target high-reduction potential substrates (Hi) through its LRET pathway (denoted with red arrows) to form either Compound II*a* or II*b*. From Compound II*a*, manganese or a low-reduction potential substrate can be oxidized, or an additional high-reduction potential substrate can be oxidized by Compound II*b* (iron (III)-Trp radical) to return the enzyme to its resting state.

(Hammel and Cullen, 2008; Pérez-Boada et al., 2005). Alternatively, in the presence of hydrogen peroxide the VP's LRET oxidation pathway is activated, allowing the enzyme to directly target high-reduction potential and bulky substrates (Hammel and Cullen, 2008; Pérez-Boada et al., 2005). The presence of this oxidation pathway facilitates VP's high-reduction potential and is one factor in differentiating its catalytic strength from that of general peroxidases. The other key factor in the high-reduction potential of VP is that its heme-iron is more electron-deficient than is found in general peroxidases, enabling VP to act as a stronger oxidant (Hammel and Cullen, 2008; Millis et al., 1989; Pérez-Boada et al., 2005). The electron-deficiency of the heme-iron is largely due to the amino acid composition of VP's heme coordination pocket and is predominantly influenced by the strength of the hydrogen bond it shares with a proximal histidine residue, resulting in a pentacoordinate ferric state (Banci et al., 1991; Camarero et al., 1999; Pérez-Boada et al., 2005).

A major limiting factor in the industrial application of VPs is that, despite their high oxidative ability and substrate versatility, they function under a narrow range of *in vitro* conditions and display reduced stability at their optimal pH (pH 3–4) (Saez-Jimenez et al., 2015b). Thus, the range of their application and cost efficiency of their use is greatly diminished (Ayala et al., 2008; Martinez et al., 2009). The optimal temperature and pH ranges of VPs are a function of their specific structural features (Fernandez-Fueyo et al., 2014b), and correspondingly, engineering a VP's optimal temperature and pH ranges requires consideration of many structural aspects. Previous engineering endeavors have been directed at improving VP pH optimality through directed evolution (Saez-Jimenez et al., 2016) and rational design (Fernandez-Fueyo et al., 2014a; Saez-Jimenez et al., 2015b), targeting surface residues far from the VP oxidation pathways and leaving the catalytic components largely unaltered. In contrast to these methods, we describe a structure-guided approach to the rational design of a peroxidase, utilizing the overall structure of one of the most temperature and pH

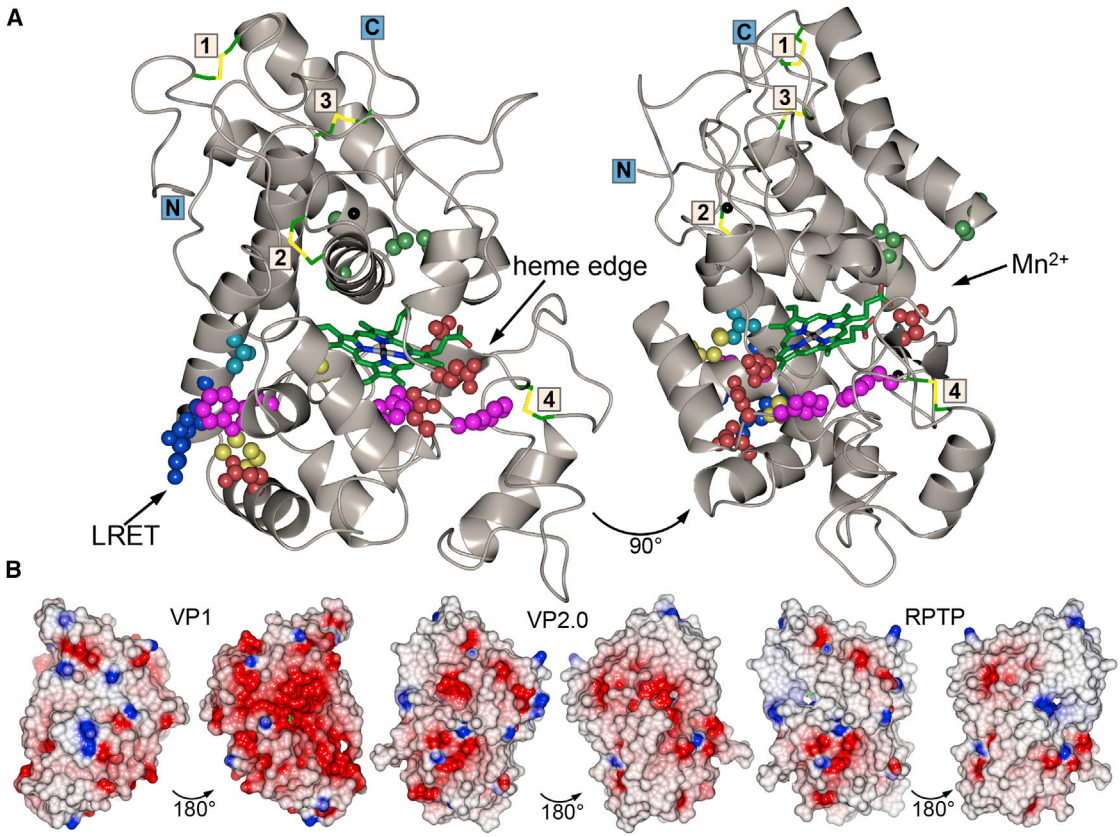

Figure 2. The Predicted Structure and Surface Properties of VP2.0

(A) The structure model of VP2.0 (gray), built from structural homology to RPTP in Phyre2 (Kelley et al., 2015), is shown coordinated with heme and two calcium ions (black spheres). VP2.0's four disulfide bridges are displayed and numbered according to their location within the VP2.0 sequence, 1–4. The 16 point mutations required to complete its oxidation pathways and heme coordination pocket are colored according to their residue properties: magenta, aromatic; green, non-polar; cyan, polar; blue, basic; red, acidic; gold, sulfur-containing.

(B) The electrostatic surface potentials of VP1, VP2.0, and RPTP are shown (red, −1 charge; blue, +1 charge). VP2.0 contains 30% fewer acidic residues compared with VP1 (28 in VP2.0 versus 40 in VP1), and consequently, the theoretical pI of VP2.0 (pI = 4.64) falls between that of VP1 (pI = 4.42) and RPTP (pI = 5.13). In addition, VP2.0 has a more even charge distribution across its surface, a trait it shares with RPTP, and in contrast, an entire face of VP1 carries a predominantly negative charge. Additional design details can be found in Figure S1.

tolerant heme peroxidases, the royal palm tree peroxidase (RPTP) from *Roystonea regia* (Sakharov et al., 2001), as a structural scaffold into which the VP catalytic components from *Pleurotus ostreatus* were built. This engineered peroxidase, VP2.0, combines the unique properties of these two enzymes—the catalytic versatility to oxidize manganese and low- and high-reduction potential substrates and activity over wider ranges of temperature (10–70°C) and pH (pH 3–7)—enabling it to outperform its VP parent.

RESULTS

Structure-guided Design of VP2.0

Pleurotus ostreatus VP1 is one of the most structurally and biochemically well-characterized VPs (Fernandez-Fueyo et al., 2014b), making it an ideal candidate to serve as the catalytic parent and model for VP2.0's heme coordination pocket and oxidation pathways. VP1's heme coordination pocket is predominantly hydrophobic and contains three key functional residues. His170 is important for pentacoordination of the heme-iron, and His40 and Arg44 catalyze the heterolytic cleavage of the oxygen-oxygen bond in hydrogen peroxide to stimulate reaction progression (Rodriguez-Lopez et al., 2001). VP1's exposed heme edge is well-conserved among heme peroxidases (Smith and Veitch, 1998), and in VP1, this site is composed of Pro77, Ala78, Ala80, Glu141, Pro142, Phe143, Lys177, Val178, and Lys216. Glu141 is predicted to control the interaction of substrates with heme, either promoting or preventing interactions depending on its orientation (Morales et al., 2012) (Figure 1A). The flanking residues contribute to the size and local charge of the site, and the geometry of their configuration in VP1 is wide enough to allow single-ring aromatics to interact directly with heme (Morales et al., 2012). The manganese site of VP1 utilizes Glu37, Glu41, and Asp176 to coordinate manganese, and sits on the enzyme surface in close proximity to the heme-proprionate group (Fernandez-Fueyo et al., 2014b) (Figure 1B). Finally, VP1's LRET pathway directly involves a surface-exposed tryptophan (Trp165) and a neighboring Leu166 to facilitate substrate oxidation (Fernandez-Fueyo et al., 2014b). Glu244 and Glu162 create an electronegative local environment around

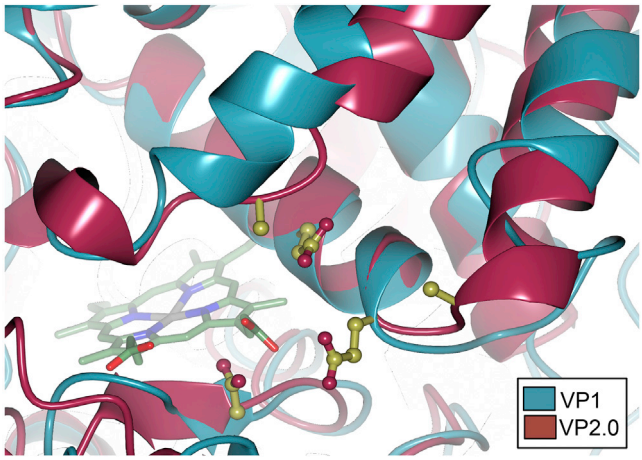

Figure 3. The Design of VP2.0's Manganese Oxidation Site

Although VP2.0 (cyan) and VP1 (red) align with an RMSD of 1.79 Å over the majority of their structures (210 residues), there are slight structural differences between the two enzymes through their manganese oxidation sites (displayed). RPTP does not contain a manganese oxidation site, so VP2.0's site was created by making the following residue substitutions: D29A, G31E, G35E, R75A, and V173D (labeled, shown in gold). Arg75 sat directly between the heme and potential manganese site and its presence was suspected to hinder heme access, so it was mutated to an alanine to mitigate this possibility. In VP1, this site is formed by two α helices and a connecting loop, while in VP2.0, this loop is replaced by an extended β-strand. The two glutamates involved in manganese interaction reside on one of the α helices, and the aspartate sits on the connecting loop in VP1 and on the β strand in VP2.0. The second α helix in VP1 extends further over the top of the oxidation site compared with that of VP2.0, and this combination of increased rigidity at the top and increased flexibility at the bottom of the site might enable VP1 to more productively coordinate manganese, better facilitating oxidation and release. These differences may contribute to VP2.0's decreased manganese oxidation activity compared with VP1, and construction of a more functional manganese site in VP2.0 may necessitate further engineering of the local secondary and tertiary structure of RPTP.

Trp165, which stabilizes the reactive cation radical state of Trp165, and Glu244 further stabilizes the radical by forming a hydrogen bond with the tryptophan indole ring nitrogen (Pérez-Boada et al., 2005). This region, from the enzyme surface to the heme coordination pocket, is also lined by Val161, Glu162, Val164, Ser169, Met248, Arg258, and Met263 (Figure 1C).

RPTP was chosen as a structural scaffold for VP2.0 because it displays thermal stability on par with that of thermophilic microbial enzymes over a broad pH range (pH 2.8–10.3) (Watanabe et al., 2010; Zamorano et al., 2008). VP1 and RPTP share only 18% sequence identity, and further differ in location of their four disulfide bridges; number of oxidation pathways (three in VP1 versus one in RPTP); and residue composition of the enzyme surface and heme coordination pocket (Figure S1). However, VP1 and RPTP share significant structural homology, aligning over 209 residues with an RMSD of 1.76 Å. This alignment encompasses the heme and calcium coordination sites of both enzymes, which greatly facilitated the construction of VP2.0. Sixteen point mutations were introduced into RPTP to complete the oxidation pathways and heme pocket and to minimize any suspected steric hindrances due to the introduction of these new functional residues (Figures 2 and S1C). Three mutations (F152M, L222F, A270K) were required to complete the heme coordination site of VP2.0 because the key functional residues and overall hydrophobic character of the site were conserved between VP1 and RPTP (Watanabe et al., 2010). The exposed heme edge architecture was also conserved between these enzymes, and this site required S140E, L142F, and F143D mutations to reconstitute the electrostatic and steric environment found in VP1.

The LRET pathway and manganese oxidation sites did not exist in RPTP. Therefore, mutations were introduced to construct these sites and account for the residue properties and spatial organization found in VP1. The secondary and tertiary structure of the LRET oxidation pathway location was similar between RPTP and VP1, and this enabled straightforward placement of functional residues. A surface-exposed tryptophan (T164W) was introduced at the pathway entrance, and a glutamate (A260E), responsible for stabilizing the tryptophan, was placed at hydrogen bond distance to the tryptophan indole nitrogen. Additional mutations (K274R, N264M, A278T) were made to complete the electronic and steric character of this pathway. The manganese oxidation site was the most challenging to engineer because VP1 and RPTP differ in residue composition and architecture through this region. This site was constructed in the same location relative to the heme-proprionate group as found in VP1 and special attention to functional residue placement was required to maintain proper geometry for manganese coordination (Figure 3). In VP1, manganese is coordinated by interactions with three carboxylate groups (Ruiz-Duenas et al., 2009), and these were introduced with G31E, G35E, and V173D mutations. Glutamate mutations at Gly31 and Gly35 align well with Glu37 and Glu41 in VP1, but placement of the aspartate was more challenging as Asp176 sits on a flexible connecting loop in VP1, while the equivalent position in RPTP is located on a β strand and placed the aspartate too far from Glu35 (Figure 3). To maintain similar distances between these residues, aspartate was placed at Val173, 5 Å from Glu35, mimicking the equivalent distance in VP1 (4.2 Å) as closely as possible given the local RPTP structure. Two additional mutations (N29A, R75A) were required to complete this site. RPTP's calcium coordination sites and disulfide bridge locations were preserved in the VP2.0 design.

VP2.0's Catalytic Versatility and Ability to Target High-Reduction Potential Substrates Is Comparable with that of VP1

To compare the catalytic versatility of VP2.0 with that of its catalytic parent, the ability of each enzyme to oxidize typical VP substrates was evaluated under the optimal conditions reported for VP1 (Fernandez-Fueyo et al., 2014b) (Figure 4A). The exposed heme edge traditionally targets low-reduction potential substrates, such as 2,2′-azino-bis(3-ethylbenzothiazoline-6-sulfonic acid) (ABTS) and 2,6-dimethylphenol (DMP), and this site functions similarly in VP2.0 and VP1 as both displayed relatively equivalent activity on these substrates (Figure 4A). Both enzymes exhibited strong oxidation activity on ABTS, and both showed similar, though reduced, activity on DMP. Functionality of the high-reduction potential LRET pathway was assessed by measuring the activity of VP2.0 and VP1 on reactive black 5 (RB5), a high-reduction potential

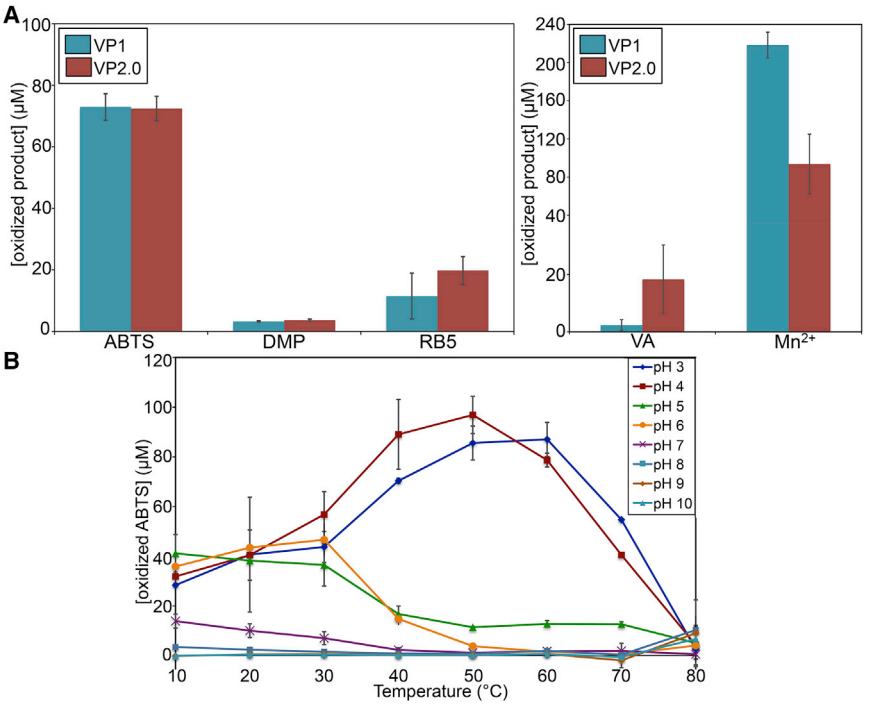

Figure 4. VP2.0 Exhibits Greater Oxidative Activity on High-Reduction Potential Substrates, Reactive Black 5 and Veratryl Alcohol

(A) The activity of VP2.0 (red) and VP1 (cyan) was assayed on five standard versatile peroxidase substrates (2,2′-azino-bis(3-ethylbenzothiazoline-6-sulfonic acid) [ABTS], 2,6-dimethylphenol [DMP], RB5, VA, and manganese [Mn^{2+}]). VP2.0 outperformed VP1 on RB5 and VA, but displayed a 60% reduction in activity on Mn^{2+} compared with VP1. Assays were performed for 2 hr at 30°C and pH 3 (ABTS, DMP, RB5, VA) and at pH 5 for Mn^{2+}. Reactions were performed in triplicate and data shown are mean ± sample standard deviation (black bars). ABTS, DMP, and RB5 were assayed with 0.06 U of enzyme (left graph) and higher reduction potential substrates (VA, Mn^{2+}) were assayed with 0.25 U of enzyme (right graph).

(B) The temperature and pH profile of VP2.0-catalyzed ABTS oxidation. Reactions were run in duplicate and data shown is mean ± sample standard deviation (black bars). VP1's temperature and pH profile are presented in Figure S2.

dye (Fernandez-Fueyo et al., 2014b), and veratryl alcohol (VA), a non-phenolic aromatic targeted exclusively by the LRET pathway (Morales et al., 2012). Although both VP2.0 and VP1 were active on RB5, VP2.0 slightly outperformed VP1 on this substrate, and significantly outperformed VP1 on VA, oxidizing roughly 90% more VA (Figure 4A).

Because VP2.0's manganese site was the most difficult to engineer, the enzyme's ability to oxidize manganese was of great interest in evaluating the success of its design. To assess VP2.0's manganese oxidation activity, the formation of the manganese (III)-malonate product was measured at the optimal pH for VP1 manganese oxidation (pH 5) (Fernandez-Fueyo et al., 2014b; Popp and Kirk, 1991). VP2.0 displayed manganese oxidation activity, albeit with approximately 60% lower activity than was measured for VP1 (Figure 4A). Given the difference in oxidation site architecture between VP1 and RPTP and RPTP's inability to oxidize manganese, it is promising that VP2.0 displayed activity on manganese, and this decreased activity when compared with VP1 may result from imprecise manganese coordination geometry and reduced ability to initially bind or release manganese upon oxidation. In stark contrast to VP2.0, RPTP is only active on low-reduction potential substrates (ABTS and ferulic acid) and is incapable of VA oxidation (Sakharov et al., 2001). Thus, from a catalytic viewpoint, the design of VP2.0 succeeded in reconstructing the key catalytic components of VP1 into the RPTP structural scaffold, producing a peroxidase capable of oxidizing low and high-reduction potential substrates in addition to manganese.

VP2.0 Exhibits Activity Over Broader Temperature and pH Ranges

To better understand the conditions necessary for fundamental peroxidase activity of VP2.0 and VP1, the ability of these enzymes to oxidize ABTS was assessed over a range of temperature and pH conditions (10–80°C, in 10°C steps and pH 3–10) (Figures 4B and S2). VP2.0 achieved its maximal oxidation activity at pH 3–4 and 40–50°C, and exhibited reduced, but measurable, activity at pH 5–7 and temperatures from 10 to 30°C (Figure 4B and Table 1). The temperature at which the activity of VP2.0 dropped to 50% of its maximum ($T_{50,\ activity}$) occurred at 72.2°C (pH 3) and 68°C (pH 4) (Table 1). Similarly, VP1 displayed $T_{50,activity}$ values of 73.5°C (pH 3) and 68.6°C (pH 4). To evaluate the ability of these enzymes to maintain their activity with extended exposure to these temperature and pH ranges, the peroxidases were subjected to a 1-hr incubation at each temperature and pH condition described above (Figure 5A). Under this experimental design, VP2.0 dramatically outperformed its catalytic parent, as its $T_{50,\ activity}$ values were relatively unaltered at its optimal pH (pH 3–4), while VP1's $T_{50,\ activity}$ decreased by 40°C at pH 3–4 (Figures 5A, S3, and Table 1). VP1 exhibited a significant change in its temperature and pH profile upon extended incubation under these conditions. At its optimal pH (pH 3), VP1's optimal temperature shifted dramatically to 10°C, and above pH 4, it was inactive at all assayed temperatures (Figure S3B). VP2.0 also exhibited a change in its temperature and pH profile with extended incubation, displaying a shift in optimal temperature to 60°C at pH 3, and reduced activity at pH 4 relative to pH 3 but with no significant change in optimal temperature (Figure S3A). In contrast to VP1, the activity of VP2.0 was relatively unaffected by incubation at pH 5–7 and temperature from 10 to 30°C.

Length of incubation, or the amount of time spent under stress, had a substantial effect on the residual activity of VP2.0 and VP1 (Figure 5B). After 1 min of incubation at their optimal temperature and pH, VP1 had lost 75% of its activity and VP2.0's activity was reduced by 48%. After 1 hr of incubation, the activity of VP1 had

Table 1. Temperature and pH Values for VP2.0 and VP1 ABTS Activity

	T_{opt}	pH_{opt}	$T_{50,\ activity}$ (pH 3)	$T_{50,\ activity}$ (pH 4)	Pretreat $T_{50,\ activity}$ (pH 3)	Pretreat $T_{50,\ activity}$ (pH 4)
VP2.0	40–50°C	pH 3–4	72.2°C ± 0.5°C	68°C ± 1.2°C	79.3°C ± 1.1°C	73.6°C ± 3.0°C
VP1	40–50°C	pH 3–4	73.5°C ± 0.2°C	68.6°C ± 1.2°C	33.5°C ± 1.9°C	33.8°C ± 7.6°C

T_{opt} and pH_{opt} are the optimal temperature and pH for enzymatic activity, and $T_{50,activity}$ is the temperature at which the enzyme functions at 50% of its maximal activity. The $T_{50,\ activity}$ values for VP2.0 and VP1 without pre-incubation at pH 3 and pH 4 and with pre-incubation (denoted "pretreat") are provided as mean values ± sample standard deviation. T_{opt}, pH_{opt}, and $T_{50,activity}$ values were calculated from data shown in Figures 3 and S2 (performed in duplicate) and pretreat $T_{50,activity}$ values were calculated from data presented in Figure S3 (performed in triplicate).

dropped by 83% while VP2.0 experienced a 53% decrease in residual activity. It is not surprising that both enzymes exhibited a decrease in residual activity with prolonged incubation under their optimal reaction conditions as enzyme instability at acidic pHs and/or increased temperatures has been observed for both VPs and lignin peroxidases (Fernandez-Fueyo et al., 2014a; Taboada-Puig et al., 2011; Tuisel et al., 1990). Thus, these results suggested that, compared with VP1, VP2.0 had an enhanced stability and, more importantly for industrial applications, improved ability to maintain a higher residual activity across broader temperature and pH ranges compared with its catalytic parent.

VP2.0 Displays Greater Structural Stability under Optimal VP Reaction Conditions

To gain a more detailed understanding of the effect of temperature and pH on the structural stability of VP2.0 and VP1, far-UV circular dichroism (CD) spectroscopy was utilized to investigate the changes in secondary structure of these peroxidases upon temperature or pH incubation. The effect of temperature was assessed by incubating each enzyme at their optimal pH (pH 3) at temperatures ranging from 25 to 80°C. Both peroxidases exhibited far-UV CD spectra characteristic of proteins with high α-helical content (Zamorano et al., 2008). The far-UV CD spectra of VP2.0 was very similar in profile to that of RPTP (Zamorano et al., 2008), suggesting that the overall structural fold of RPTP was indeed conserved in VP2.0. Compared with VP1, VP2.0 had a wider overall trough with double minima at 208 and 222 nm (Figure 6A). As temperature increased, VP2.0's far-UV CD spectra also displayed similar behavior to that of RPTP, maintaining its characteristic profile from 25 to 65°C and the two minima became less defined as temperatures surpassed 70°C (Figures 6A and S4A). Conversely, VP1 displayed a single, distinct minimum at 208 nm at 25°C, and this minimum shifted substantially to the right as temperature increased above 35°C, reaching 215 nm at 80°C (Figures 6B and S4B). Although both enzymes demonstrated a change in secondary structure with increasing temperature, VP2.0 retained its native structure over a wider temperature range than did VP1, resisting secondary structure disruption by 30°C above the temperature at which VP1 began to exhibit structural change.

The effect of pH on structural stability was evaluated by incubating the enzymes at pH 3, 5, and 8 at their optimal temperature (50°C), and far-UV CD spectra were collected at time 0 (T0) and after 1 hr (T60) of incubation. At pH 3 and 8, VP2.0 displayed its characteristic, double minima (208, 222 nm) far-UV CD spectra profile (Figure 6C). VP2.0's minimum at 208 nm was more pronounced at pH 8 than at pH 3, and incubation under these conditions had little effect on the α-helical content of VP2.0, as indicated by minimal change in far-UV CD spectra at T0 and T60. At pH 5, VP2.0 demonstrated significant structural instability, which was evident from the large change in its far-UV CD spectra and clear loss of its defined minima (Figure 6C). In addition, prolonged incubation at pH 5 led to further secondary structure loss. Interestingly, these structural changes were not substantial enough to render VP2.0 inactive, as the enzyme was still capable of substrate oxidation at pH 5; however, this reduced stability may have contributed to VP2.0's decreased manganese activity (Figures 4 and S3A). The far-UV CD spectra of VP1 at pH 3 had a single minimum at 208 nm, and this minimum shifted to 215 nm upon prolonged incubation (Figure 6D). VP1 was minimally affected by incubation at pH 5, maintaining its minimum (208 nm) with little difference between T0 and T60 spectra. However, VP1 underwent a significant change in far-UV CD spectra at pH 8 (Figure 6D). Its minimum shifted to 204 nm and its molar ellipticity decreased substantially between 210 and 225 nm, indicating a shift from predominately α-helical content to random coil motifs (Johnson, 1990). Although both VP2.0 and VP1 were affected by pH, these analyses suggested that VP2.0 was structurally more stable than its catalytic parent under optimal reaction conditions (pH 3).

DISCUSSION

Based on far-UV CD analyses, VP2.0 exhibited greater structural stability over a broader temperature range and at acidic pH (pH 3) compared with VP1, and this enhanced stability is likely a key factor in its ability to maintain a higher residual activity when subjected to prolonged incubation at optimal reaction conditions (Figures 5 and 6). Although VP2.0 did not experience as dramatic of a drop in residual activity as did VP1, it did show a marked decrease within the first minute of incubation at pH 3 and 50°C (Figure 5B). This initial decrease is unlikely, based on lack of large structural changes as monitored by CD spectroscopy, due to significant deformation of the heme coordination site, oxidative sites, or loss of important structural elements like disulfide bridges. Instead, this loss in activity may be due to more subtle changes, such as partial disruption of the hydrogen bond interaction network present in the heme coordination site (Fernandez-Fueyo et al., 2014a), a reduction in reaction rate possibly due to changes in the heme oxidation state or the protonation states of residues involved in the oxidation pathways (Fernandez-Fueyo et al., 2014a), and/or oxidative damage of the enzyme by peroxide radical formation (Saez-Jimenez et al., 2015a). As evidenced by Figure 5B, however, these possible effects have less of an impact on the activity of VP2.0 as they do on that of VP1 – VP2.0 retains 47% of its activity after 1 hr of incubation while VP1 only retains 17% of its activity under the same conditions.

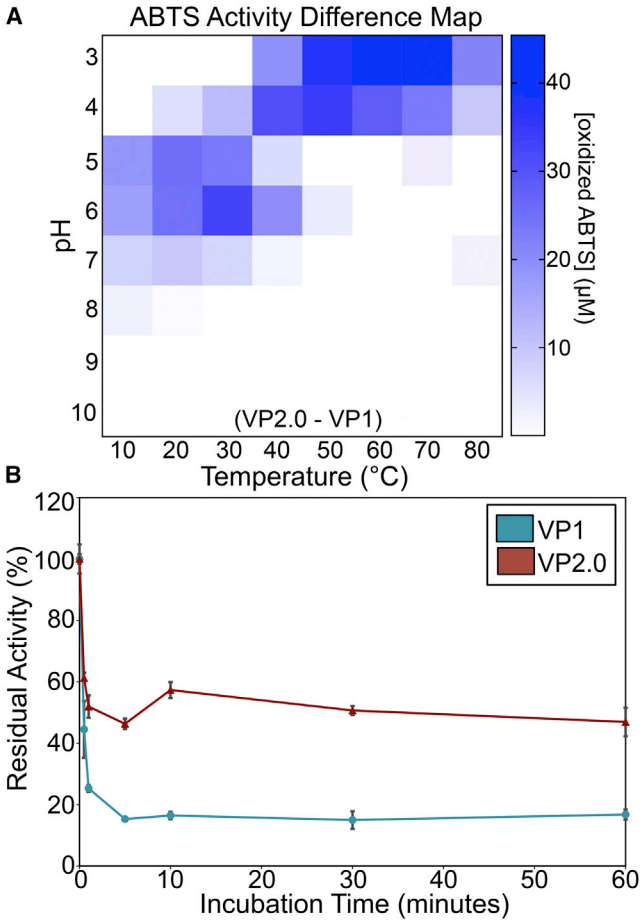

Figure 5. VP2.0 Maintains Higher Residual Activity under Temperature and pH Stress

(A) To assess the effect of temperature and pH stress on enzymatic activity, VP2.0 and VP1 were incubated for 1 hr at temperatures from 10 to 80°C, in 10°C steps, and pH from 3 to 10. ABTS and hydrogen peroxide were then added and the reaction was allowed to proceed. The difference in ABTS oxidation activity between VP2.0 and VP1 is illustrated with a difference map. Blue areas represent conditions under which VP2.0 outperformed VP1 and degree of blue shading indicates the amount of oxidized ABTS (μM) produced by VP2.0 in excess of that produced by VP1. Experiments were run in triplicate, and the resulting temperature and pH profile for each enzyme is presented in Figure S3.

(B) The effect of incubation time on residual enzyme activity was evaluated by incubating VP2.0 (red) and VP1 (cyan) at their optimal reaction conditions (50°C [pH 3]) for varying amounts of time. Reactions were then initiated with the addition of ABTS and hydrogen peroxide. Activities are provided as a percentage relative to enzyme activity without prior incubation. Assays were run in duplicate, and data shown are the means ± sample standard deviation (black bars).

The enhanced structural stability of VP2.0 is likely a product of the high-sequence homology that it shares with RPTP, enabling the engineered peroxidase to benefit from many of the structural factors that contribute to RPTP's unusually broad temperature and pH stability, such as a similar inter- and intra-molecular force profile, increased α-helical content, and structural compactness. Alteration of the surface charge distribution and more generally, alteration of residue identity throughout the enzyme, leads to changes in intra-molecular forces, such as salt bridges and hydrogen bonds, that govern secondary structural elements and overall enzyme fold. VP2.0, unlike VP1, has a relatively evenly distributed electrostatic surface potential, which may mitigate self-aggregation and have a favorable impact on its substrate and solvent interactions. VP2.0 has fewer negatively charged surface residues, and thus has an increased pI relative to VP1 (pI[VP2.0] = 4.64; pI[VP1] = 4.42). Protein solubility or stability often decreases as the solution pH approaches the protein pI, the pH at which a protein carries zero net surface charge (Golovanov et al., 2004). As the solution pH approaches its pI, a protein's surface becomes less charged and the electrostatic repulsions that typically exist between protein molecules subside, often leading to protein aggregation (Golovanov et al., 2004). Therefore, an increase in VP2.0's pI would likely increase its stability at its optimal reaction pH (pH 3–4). As evidenced by far-UV CD spectroscopy, VP2.0 was structurally stable at pH 3, but exhibited a loss of ordered structure when examined at pH 5, closer to its pI.

Disulfide bridges influence the structural stability of globular proteins (Creighton, 1988), and in heme peroxidases, they also influence calcium coordination and enzyme activity (Watanabe et al., 2010). VP2.0 shares RPTP's disulfide bridge pattern, and while the overall number of disulfides is equal between VP2.0 and VP1, the enzymes differ in spatial arrangement of their disulfide bridges (Figure S1B). The arrangement found in RPTP and VP2.0 is characteristic of secretory plant heme peroxidases, which typically display higher temperature and pH tolerance than do the fungal extracellular heme peroxidases, such as VP1 (Zamorano et al., 2008). In particular, RPTP's second disulfide bridge (Cys44-Cys49) restrains an extended loop, which is unrestrained in VP1, and enhances the structural stability of the distal calcium coordination site (Watanabe et al., 2010). Calcium coordination is important for heme peroxidase structural stability, as it aids in maintenance of proper heme coordination pocket architecture and influences thermal stability (Saez-Jimenez et al., 2015b, 2016). Although the locations and general residue composition of the calcium coordination sites are conserved between VP2.0 and VP1, it is possible that they vary in their ability to coordinate calcium due to differences in organization and strength of nearby intra-molecular interactions, especially if these interactions are variably disrupted by temperature and pH stress (Watanabe et al., 2010). These differences in disulfide bridge arrangement, and possibly calcium coordination, may be important factors in VP2.0's enhanced stability and ability to function over broader ranges of temperature and pH in comparison with VP1.

Finally, VP2.0 is predicted to have longer α helices, and consequently, 10% greater α-helical content compared with VP1. This increased α-helical content combined with tighter packing of these structural elements, as is observed in RPTP and predicted for VP2.0 (Figure S1A), may encourage a more rigid overall structure that together with other structural features, such as intra-molecular forces and calcium coordination, would enable these enzymes to better withstand harsher conditions. It is important to note that one contributing factor in RPTP stability is the presence of nine *N*-glycosylation sites (Watanabe et al., 2010), and neither VP2.0 nor VP1 are glycosylated when produced recombinantly in *E. coli* BL21(DE3) cells.

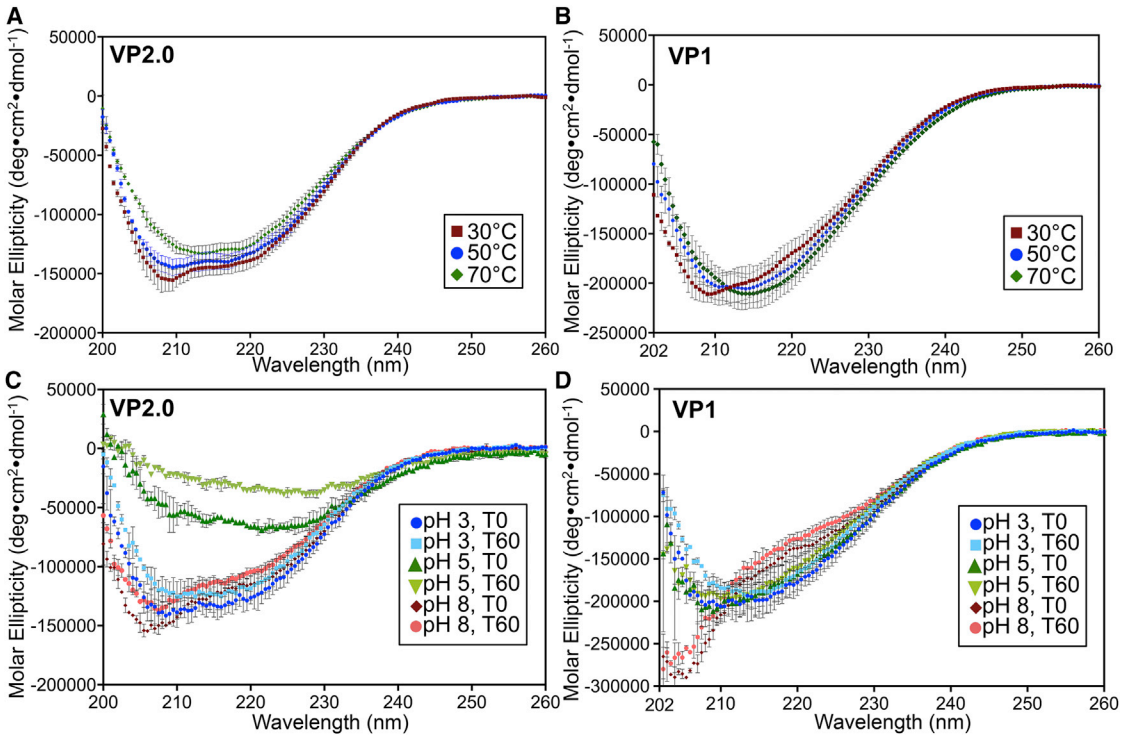

Figure 6. Far-UV CD Spectroscopy Provides Structural Insight into the Thermal and pH Stability of VP2.0

The effect of temperature on the structural stability of VP2.0 (A) and VP1 (B) was evaluated by assessing changes in secondary structure using far-UV circular dichroism (CD) spectroscopy at temperatures ranging from 25 to 80°C, in 5°C steps, at a constant pH (pH 3). Data from 30°C, 50°C, and 70°C are shown here, and complete datasets are provided in Figure S4. Both enzymes exhibit far-UV CD spectra characteristic of proteins with high α-helical content. VP2.0 was stable up to 70°C, while VP1 began to display structural instability at 40°C. The effect of pH on the structural stability of VP2.0 (C) and VP1 (D) was examined using far-UV CD spectroscopy at constant temperature (50°C) and varied pH (pH 3, 5, 8). Far-UV CD spectra were collected at time 0 (T0) and after 60 min (T60) of incubation under these conditions. VP2.0 displayed significant loss of ordered structure at pH 5 but was minimally affected by pH 3 and pH 8. Conversely, VP1 was most stable at pH 5, less stable at pH 3, and experienced significant structural change at pH 8. The far-UV CD spectra in (A)–(D) are representative of two experiments and are presented as mean molar ellipticity ± sample standard deviation (black bars).

Nevertheless, as described above, many factors that contribute to RPTP's structural stability are conserved in VP2.0, and although the exact contributions of these factors are difficult to quantify directly, their cumulative, positive effect on VP2.0 is evident in the activity profiling data and far-UV CD spectroscopy results presented here.

Since many structural features have been implicated in heme peroxidase stability, this structure-guided, rational engineering approach aimed to make substantial, global changes to a VP, combining the positive traits of related but catalytically and species diverse enzymes, to create a high-reduction potential peroxidase that would be amenable to broader industrial application. Therefore, instead of making localized mutations on VP1, we rebuilt its catalytic hardware into a more stable structural scaffold. VP2.0, the resulting peroxidase, displayed greater structural stability than its catalytic parent, and due to this stability, VP2.0 was capable of functionally withstanding extended exposure to a wider range of temperature and pH conditions. As our understanding of the structural and functional relationships governing diverse enzyme classes continues to expand, the ability to apply structure-guided design so too will follow, further enabling the direct design of industrially tailored, highly effective biocatalysts.

SIGNIFICANCE

Heme peroxidases catalyze reduction-oxidation reactions that are essential to life, and they have also gained widespread application throughout industry as they offer a much-needed, relatively mild alternative to traditional, harsh chemical catalysts. However, the potential for these enzymes is far greater than their present use, as processes are currently restricted to the more stable, but less catalytically powerful, subset of peroxidases. For instance, their potential extends to environmental remediation of emerging pollutants, such as pesticides, pharmaceuticals, and other household chemicals that accumulate in waterways and adversely affect human health. High-reduction potential heme peroxidases, as sustainable, environmentally friendly, and catalytically powerful biocatalysts, are likely to become a key component in the solution to the current and future challenges that we face as we enter into a more bio-based economy. This study describes a rational engineering approach for the direct design of innovative, industrially tailored biocatalysts. We apply this approach to address the current application barrier of high-reduction potential peroxidases as biocatalytic tools, building the catalytic

hardware of a high-reduction potential fungal peroxidase into the structural scaffold of a highly stable plant peroxidase. The resulting hybrid heme peroxidase has the catalytic versatility and oxidative ability of a high-reduction potential versatile peroxidase with the enhanced temperature and pH tolerance of a highly stable plant peroxidase.

STAR★METHODS

Detailed methods are provided in the online version of this paper and include the following:

- KEY RESOURCES TABLE
- CONTACT FOR REAGENT AND RESOURCE SHARING
- METHOD DETAILS
  - Gene and Plasmid Construction
  - Protein Expression and Purification
  - Substrate Screen Assay
  - Temperature and pH Assays
  - Circular Dichroism Spectroscopy
- QUANTIFICATION AND STATISTICAL ANALYSIS
- DATA AND SOFTWARE AVAILABILITY

SUPPLEMENTAL INFORMATION

Supplemental Information includes four figures can be found with this article online at https://doi.org/10.1016/j.chembiol.2018.04.014.

ACKNOWLEDGMENTS

This work was conducted by the Joint BioEnergy Institutes and was supported by the United States Department of Energy, Office of Science and Office of Biological and Environmental Research under contract no. DE-AC02-05CH11231.

AUTHOR CONTRIBUTIONS

Conceptualization, Methodology, and Investigation, A.C.K.; Writing – Original Draft, A.C.K.; Writing – Review & Editing, A.C.K., B.A.S., and K.L.S.; Funding Acquisition, B.A.S. and K.L.S.

DECLARATION OF INTERESTS

A.C.K., B.A.S., and K.L.S. have a patent application related to this work, which is assigned to The Regents of the University of California and National Technology & Engineering Solutions of Sandia, LLC (NTESS).

Received: November 22, 2017
Revised: March 7, 2018
Accepted: April 13, 2018
Published: May 24, 2018

REFERENCES

Ayala, M., Pickard, M.A., and Vazquez-Duhalt, R. (2008). Fungal enzymes for environmental purposes, a molecular biology challenge. J. Mol. Microbiol. Biotechnol. *15*, 172–180.

Ayala, M., and Torres, E. (2016). Peroxidases as potential industrial biocatalysts. In Heme Peroxidases, E. Raven and B. Dunford, eds. (The Royal Society of Chemistry), pp. 309–333.

Banci, L., Bertini, I., Turano, P., Tien, M., and Kirk, T.K. (1991). Proton NMR investigation into the basis for the relatively high redox potential of lignin peroxidase. Proc. Natl. Acad. Sci. USA *88*, 6956–6960.

Busse, N., and Czermak, P. (2016). Role and application of versatile peroxidase (VP) for utilizing Lignocellulose in biorefineries. In Microbial Enzymes in Bioconversions of Biomass, V.K. Gupta, ed. (Springer), pp. 271–300.

Camarero, S., Sarkar, S., Ruiz-Duenas, F.J., Martinez, M.J., and Martinez, A.T. (1999). Description of a versatile peroxidase involved in the natural degradation of lignin that has both manganese peroxidase and lignin peroxidase substrate interaction sites. J. Biol. Chem. *274*, 10324–10330.

Creighton, T.E. (1988). Disulphide bonds and protein stability. Bioessays *8*, 57–63.

de Montellano, P.R.O. (2010). Catalytic mechanisms of heme peroxidases. In Biocatalysis Based on Heme Peroxidases: Peroxidases as Potential Industrial Biocatalysts, E. Torres and M. Ayala, eds. (Springer), pp. 79–107.

Deblonde, T., Cossu-Leguille, C., and Hartemann, P. (2011). Emerging pollutants in wastewater: a review of the literature. Int. J. Hyg. Environ. Health *214*, 442–448.

Eibes, G., Debernardi, G., Feijoo, G., Moreira, M.T., and Lema, J.M. (2011). Oxidation of pharmaceutically active compounds by a ligninolytic fungal peroxidase. Biodegradation *22*, 539–550.

Fernandez-Fueyo, E., Ruiz-Duenas, F.J., and Martinez, A.T. (2014a). Engineering a fungal peroxidase that degrades lignin at very acidic pH. Biotechnol. Biofuels *7*, 114.

Fernandez-Fueyo, E., Ruiz-Duenas, F.J., Martinez, M.J., Romero, A., Hammel, K.E., Medrano, F.J., and Martinez, A.T. (2014b). Ligninolytic peroxidase genes in the oyster mushroom genome: heterologous expression, molecular structure, catalytic and stability properties, and lignin-degrading ability. Biotechnol. Biofuels *7*, 2.

Golovanov, A.P., Hautbergue, G.M., Wilson, S.A., and Lian, L.Y. (2004). A simple method for improving protein solubility and long-term stability. J. Am. Chem. Soc. *126*, 8933–8939.

Hammel, K.E., and Cullen, D. (2008). Role of fungal peroxidases in biological ligninolysis. Curr. Opin. Plant Biol. *11*, 349–355.

Isaac, I.S., and Dawson, J.H. (1999). Haem iron-containing peroxidases. Essays Biochem. *34*, 51–69.

Johnson, W.C., Jr. (1990). Protein secondary structure and circular dichroism: a practical guide. Proteins *7*, 205–214.

Kelley, L.A., Mezulis, S., Yates, C.M., Wass, M.N., and Sternberg, M.J. (2015). The Phyre2 web portal for protein modeling, prediction and analysis. Nat. Protoc. *10*, 845–858.

Kelly, S.M., Jess, T.J., and Price, N.C. (2005). How to study proteins by circular dichroism. Biochim. Biophys. Acta *1751*, 119–139.

Knop, D., Levinson, D., Makovitzki, A., Agami, A., Lerer, E., Mimran, A., Yarden, O., and Hadar, Y. (2016). Limits of versatility of versatile peroxidase. Appl. Environ. Microbiol. *82*, 4070–4080.

Martinez, A.T., Ruiz-Duenas, F.J., Martinez, M.J., Del Rio, J.C., and Gutierrez, A. (2009). Enzymatic delignification of plant cell wall: from nature to mill. Curr. Opin. Biotechnol. *20*, 348–357.

Millis, C.D., Cai, D.Y., Stankovich, M.T., and Tien, M. (1989). Oxidation-reduction potentials and ionization states of extracellular peroxidases from the lignin-degrading fungus *Phanerochaete chrysosporium*. Biochemistry *28*, 8484–8489.

Morales, M., Mate, M.J., Romero, A., Martinez, M.J., Martinez, A.T., and Ruiz-Duenas, F.J. (2012). Two oxidation sites for low redox potential substrates: a directed mutagenesis, kinetic, and crystallographic study on *Pleurotus eryngii* versatile peroxidase. J. Biol. Chem. *287*, 41053–41067.

Notredame, C., Higgins, D.G., and Heringa, J. (2000). T-Coffee: a novel method for fast and accurate multiple sequence alignment. J. Mol. Biol. *302*, 205–217.

Pérez-Boada, M., Doyle, W.A., Ruiz-Duenas, F.J., Martinez, M.J., Martinez, A.T., and Smith, A.T. (2002). Expression of *Pleurotus eryngii* versatile peroxidase in *Escherichia coli* and optimisation of in vitro folding. Enzyme Microb. Technol. *30*, 7.

Pérez-Boada, M., Ruiz-Duenas, F.J., Pogni, R., Basosi, R., Choinowski, T., Martinez, M.J., Piontek, K., and Martinez, A.T. (2005). Versatile peroxidase oxidation of high redox potential aromatic compounds: site-directed mutagenesis, spectroscopic and crystallographic investigation of three long-range electron transfer pathways. J. Mol. Biol. *354*, 385–402.

Popp, J.L., and Kirk, T.K. (1991). Oxidation of methoxybenzenes by manganese peroxidase and by Mn^{3+}. Arch. Biochem. Biophys. *288*, 145–148.

Rodriguez-Lopez, J.N., Lowe, D.J., Hernandez-Ruiz, J., Hiner, A.N., Garcia-Canovas, F., and Thorneley, R.N. (2001). Mechanism of reaction of hydrogen peroxide with horseradish peroxidase: identification of intermediates in the catalytic cycle. J. Am. Chem. Soc. *123*, 11838–11847.

Ruiz-Duenas, F.J., Morales, M., Garcia, E., Miki, Y., Martinez, M.J., and Martinez, A.T. (2009). Substrate oxidation sites in versatile peroxidase and other basidiomycete peroxidases. J. Exp. Bot. *60*, 441–452.

Saez-Jimenez, V., Acebes, S., Garcia-Ruiz, E., Romero, A., Guallar, V., Alcalde, M., Medrano, F.J., Martinez, A.T., and Ruiz-Duenas, F.J. (2016). Unveiling the basis of alkaline stability of an evolved versatile peroxidase. Biochem. J. *473*, 1917–1928.

Saez-Jimenez, V., Acebes, S., Guallar, V., Martinez, A.T., and Ruiz-Duenas, F.J. (2015a). Improving the oxidative stability of a high redox potential fungal peroxidase by rational design. PLoS One *10*, e0124750.

Saez-Jimenez, V., Fernandez-Fueyo, E., Medrano, F.J., Romero, A., Martinez, A.T., and Ruiz-Duenas, F.J. (2015b). Improving the pH-stability of versatile peroxidase by comparative structural analysis with a naturally-stable manganese peroxidase. PLoS One *10*, e0140984.

Sakharov, I.Y., Vesga, M.K., Galaev, I.Y., Sakharova, I.V., and Pletjushkina, O.Y. (2001). Peroxidase from leaves of royal palm tree *Roystonea regia*: purification and some properties. Plant Sci. *161*, 853–860.

Smith, A.T., and Veitch, N.C. (1998). Substrate binding and catalysis in heme peroxidases. Curr. Opin. Chem. Biol. *2*, 269–278.

Taboada-Puig, R., Junghanns, C., Demarche, P., Moreira, M.T., Feijoo, G., Lema, J.M., and Agathos, S.N. (2011). Combined cross-linked enzyme aggregates from versatile peroxidase and glucose oxidase: production, partial characterization and application for the elimination of endocrine disruptors. Bioresour. Technol. *102*, 6593–6599.

Tuisel, H., Sinclair, R., Bumpus, J.A., Ashbaugh, W., Brock, B.J., and Aust, S.D. (1990). Lignin peroxidase H2 from *Phanerochaete chrysosporium*: purification, characterization and stability to temperature and pH. Arch. Biochem. Biophys. *279*, 158–166.

Watanabe, L., de Moura, P.R., Bleicher, L., Nascimento, A.S., Zamorano, L.S., Calvete, J.J., Sanz, L., Perez, A., Bursakov, S., Roig, M.G., et al. (2010). Crystal structure and statistical coupling analysis of highly glycosylated peroxidase from royal palm tree (*Roystonea regia*). J. Struct. Biol. *169*, 226–242.

Wen, X., Jia, Y., and Li, J. (2009). Degradation of tetracycline and oxytetracycline by crude lignin peroxidase prepared from *Phanerochaete chrysosporium*–a white rot fungus. Chemosphere *75*, 1003–1007.

Zamocky, M., Hofbauer, S., Schaffner, I., Gasselhuber, B., Nicolussi, A., Soudi, M., Pirker, K.F., Furtmuller, P.G., and Obinger, C. (2015). Independent evolution of four heme peroxidase superfamilies. Arch. Biochem. Biophys. *574*, 108–119.

Zamorano, L.S., Pina, D.G., Arellano, J.B., Bursakov, S.A., Zhadan, A.P., Calvete, J.J., Sanz, L., Nielsen, P.R., Villar, E., Gavel, O., et al. (2008). Thermodynamic characterization of the palm tree *Roystonea regia* peroxidase stability. Biochimie *90*, 1737–1749.

STAR★METHODS

KEY RESOURCES TABLE

REAGENT or RESOURCE	SOURCE	IDENTIFIER
Bacterial and Virus Strains		
E. coli BL21(DE3)	New England Biolabs, Inc.	Cat. No. C25271
Chemicals, Peptides, and Recombinant Proteins		
2,2'-azino-bis(3-ethylbenzothiazoline-6-sulphonic acid	Sigma-Aldrich	Cat. No. A1888
Reactive Black 5	Sigma-Aldrich	Cat. No. 306452
2,6-dimethylphenol	Sigma-Aldrich	Cat. No. D174904
veratryl alcohol (3,4-dimethoxybenzyl alcohol)	Sigma-Aldrich	Cat. No. D133000
manganese sulfate	Sigma-Aldrich	Cat. No. 221287
hydrogen peroxide	Sigma-Aldrich	Cat. No. 95321
VP1	This paper	N/A
VP2.0	This paper	N/A
Recombinant DNA		
pET-28a(+)	Novagen-EMD Millipore	Cat. No. 69864
pET-28a(+)-VP1	This paper; GenScript	N/A
pET-28a(+)-VP2.0	This paper; GenScript	N/A
Deposited Data		
VP2.0 nucleotide and amino acid sequences	This paper	NCBI GenBank Accession No. MG252476
Crystal structure of *P. ostreatus* VP1	Fernandez-Fueyo et al., 2014b	PBD ID: 4BLL
Crystal structure of *R. regia* RPTP	Watanabe et al., 2010	PBD ID: 3HDL
Software and Algorithms		
Phyre2	Kelley et al., 2015	http://www.sbg.bio.ic.ac.uk/phyre2/html/page.cgi?id=index
T-Coffee	Notredame et al., 2000	http://tcoffee.crg.cat/#

CONTACT FOR REAGENT AND RESOURCE SHARING

Further information and requests for resources and reagents should be directed to and will be fulfilled by the Lead Contact, Kenneth L. Sale (klsale@sandia.gov).

METHOD DETAILS

Gene and Plasmid Construction

Full-length *P. ostreatus* versatile peroxidase (999 bp) (VP1) (GenBank: ALD10061.1) and VP2.0 (915 bp) genes were codon optimized for expression in *Escherichia coli*, synthesized (GenScript), and cloned into the pET-28a(+) expression vector (Novagen-EMD Millipore) between the NheI and NotI restriction sites. The nucleotide and amino acid sequences for the synthetic construct VP2.0 were deposited in the NCBI GenBank (https://www.ncbi.nlm.nih.gov/genbank/) (Accession No. MG252476). Amino acid sequence alignments were generated in T-coffee (Notredame et al., 2000).

Protein Expression and Purification

The pET-28a(+)-VP2.0 and pET-28a(+)-VP1 vectors were each transformed into *Escherichia coli* BL21(DE3) cells (New England Biolabs, Inc.), and cells were grown in Miller's LB media at 37°C to an OD_{600} of 0.8-1.0. Protein expression was induced by the addition of 1 mM isopropyl β-D-1-thiogalactopyranoside (IPTG) for 16 hours at 19°C. Cells were harvested by centrifugation (10 minutes at 4,000 rpm), resuspended in 50 mM Tris, pH 8.0, 250 mM sodium chloride, and 0.1 mM phenylmethylsulfonyl fluoride (PMSF), and lysed via homogenization. The homogenized cell mixture was centrifuged (40 minutes at 10,000 rpm) to separate soluble protein material from membrane-associated protein material. The soluble protein material (supernatant) was discarded and the membrane-associated material (pellet) was resuspended in 50 mM Tris, pH 8.0, 250 mM sodium chloride, 5 mM imidazole, and 8 M urea. The solubilized material was centrifuged to remove any remaining cell debris (40 minutes at 10,000 rpm), and the resulting

supernatant was applied to Ni-NTA resin (Qiagen) at room temperature (approximately 22°C). The protein was eluted from the resin in 50 mM Tris, pH 8.0, 250 mM sodium chloride, 500 mM imidazole, and 8 M urea.

The denatured, purified VP2.0 and VP1 proteins were refolded *in vitro* using a dialysis refolding method modified from that described by Pérez-Boada et al. (2002). Dialysis was performed at room temperature, in the dark, with gentle stirring for approximately 20 hours. The dialysis buffer contained: 5 mM calcium chloride, 0.5 mM oxidized glutathione, 0.1 mM 1,4-dithiothreitol, 0.16 M urea, 20 μM hemin, and 20 mM Tris, pH 9.5. Both proteins were diluted using the dialysis buffer to a concentration of 0.1-0.2 mg/mL prior to refolding and the ratio of protein volume to dialysis buffer volume was maintained at a 1:18 ratio. Post-dialysis, refolded VP2.0 and VP1 were loaded directly onto a HiTrap Q HP anion exchange column (GE Healthcare) that was equilibrated in 10 mM sodium tartrate, pH 5.5 and 1 mM calcium chloride at a 1 mL/minute load rate. Protein was eluted from the column using a sodium chloride gradient from 0-1 M run at 2 mL/min over 60 minutes. Both VP2.0 and VP1 eluted from the anion exchange column at a sodium chloride concentration of approximately 400-500 mM. As a final purification step, VP2.0 and VP1 were purified by size-exclusion chromatography using a Superdex 200 HiLoad 16/600 column (GE Healthcare) into a final buffer of 10 mM sodium tartrate, pH 5.5, 200 mM sodium chloride, 1 mM calcium chloride. Protein was flash-frozen and stored at −80°C.

Substrate Screen Assay

For all enzymatic assays with VP2.0 and VP1, Units (U) are defined as the amount of enzyme that produces 1 nmol of oxidized 2,2′-azino-bis(3-ethylbenzothiazoline-6-sulphonic acid (ABTS) per minute at 30°C and pH 3. To assess the ability of VP2.0 and VP1 to oxidize substrates of varying redox potential, each enzyme was incubated with either ABTS, Reactive Black 5 (RB5), 2,6-dimethylphenol (DMP), veratryl alcohol (VA), or manganese for 2 hours at 30°C. To measure enzyme activity on ABTS and DMP each reaction contained 0.06 U of enzyme, 5 mM hydrogen peroxide, 1 mM substrate (ABTS or DMP), and 50 mM sodium tartrate, pH 3. To determine enzyme activity on RB5, reactions contained 0.06 U of enzyme, 0.2 mM RB5, and 5 mM hydrogen peroxide, and 50 mM sodium tartrate, pH 3. For VA oxidation, reactions contained 0.25 U of enzyme, 1 mM VA, 5 mM hydrogen peroxide, and 50 mM sodium tartrate, pH 3. ABTS, DMP, RB5, and VA assays were adapted from protocols described by Fernandez-Fueyo, et al. (2014b). A protocol similar to that described by Popp and Kirk (1991) was used to assess enzyme activity on manganese, and the reaction contained 0.25 Units of VP2.0 or VP1, 20 mM sodium malonate, pH 5, 10 mM manganese sulfate, and 1 mM hydrogen peroxidase. The formation of the oxidized product was determined for each reaction by measuring the change in absorbance at the following wavelengths (product measured in parentheses): 436 nm (ABTS cation radical), 598 nm (disappearance of RB5), 469 nm (dimeric coerulignone), 310 nm (veratraldehyde), 266 nm (formation of Mn(III)-malonate complex) (Fernandez-Fueyo et al., 2014b; Popp and Kirk, 1991). Background absorbance due to the enzyme, buffer, and substrates was subtracted from the raw absorbances, and product concentrations were calculated from the resulting absorbance values using the following molar extinction coefficients: ε_{436} = 29.3 mM^{-1} cm^{-1}, ε_{598} = 30 mM^{-1} cm^{-1}, ε_{469} = 55 mM^{-1} cm^{-1}, ε_{310} = 9.3 mM^{-1} cm^{-1}, ε_{266} = 11.5 mM^{-1} cm^{-1} (Fernandez-Fueyo et al., 2014b; Popp and Kirk, 1991). Enzyme reactions were run in triplicate, and all spectroscopic assays were performed on a SpectraMax Plus 384 spectrophotometer (Molecular Devices, Sunnyvale, CA).

Temperature and pH Assays

The temperature and pH profiles for VP and VP2.0 were determined by measuring the ability of each enzyme to catalyze oxidization of ABTS under temperatures ranging from 10°C to 80°C (measured in 10°C increments) and pH ranging from pH 3-10 (measured in 1 pH unit steps). Each reaction contained 0.04 U of either VP1 or VP2.0, 1 mM calcium chloride, 1 mM ABTS, 5 mM hydrogen peroxide, 50 mM buffer agent. The buffering agents included: citric acid pH 3 and 4, sodium malonate pH 5, citric acid pH 6, tris(hydroxymethyl) aminomethane (Tris) pH 7 and 8, and *N*-cyclohexyl-2-aminoethanesulfonic acid (CHES) pH 9 and 10. Reactions were incubated for 2 hours and the concentration of oxidized ABTS was determined from the sample absorbance collected at 436 nm. Temperature and pH profile assays were performed in duplicate. For the temperature and pH pre-incubation experiment, 0.04 Units of VP1 or VP2.0 in 1 mM calcium chloride, and 50 mM buffering agent (described above) were incubated at 10°C to 80°C (in 10°C steps) for 1 hour. 1 mM ABTS and 5 mM hydrogen peroxide was then added to each reaction and the samples were incubated again at their respective temperatures for another hour. The concentration of oxidized ABTS was determined as described above. For both experiments, the background absorbance due to enzyme, buffer, and substrates was subtracted from the raw absorbances, and concentration of oxidized ABTS was determined from the molar extinction coefficient: ε_{436} = 29.3 mM^{-1} cm^{-1}. The temperature and pH pre-incubation assay was performed in triplicate.

For the time course experiment, 0.06 Units of VP2.0 and VP1 were incubated in 50 mM citric acid pH 3 at 50°C and time point aliquots were taken after 0, 0.5, 1, 5, 10, 30, and 60 minutes of incubation at 50°C. Time point reactions were initiated upon addition of 1 mM ABTS and 5 mM hydrogen peroxide, and reactions were allowed to proceed at 50°C for 1 hour. The concentration of oxidized ABTS was determined as detailed for the temperature and pH profile experiment, and the background absorbance due to the presence of enzyme, buffer, and substrates was subtracted from the raw absorbance values. Experiments were run in duplicate.

Circular Dichroism Spectroscopy

Circular dichroism (CD) spectra were acquired with a Jasco J-815 spectropolarimeter (JASCO, Maryland, USA) that was equipped with a Peltier temperature controller. For the temperature interval spectra, each sample contained 20 μM of enzyme prepared in 10 mM citric acid buffer (pH 3). Scans were performed in a 1 mm path length cell from 300 to 190 nm with a data pitch of 0.5 nm and a 1 nm bandwidth. The temperature was varied from 25°C to 80°C, in 5°C intervals, and samples were incubated at each

temperature for 60 seconds before data collection. This delay in data acquisition was based on the time course findings that the majority of activity loss occurred within a one-minute incubation, thus measurements were expected to reflect structural changes, if present. The scanning speed was 50 nm/minute with a ramp rate of 40°C/hour. Scans were performed in duplicate for each enzyme and pH. The spectra for the buffer alone (10 mM citric acid pH 3) was subtracted from the sample spectra and the resulting data was smoothed using the Jasco Spectra Manager v.2 software (JASCO, Easton, MD). Raw ellipticity (θ_{obs}) values were converted to mean residue ellipticity (θ_{molar}) using the following equation:

$$\theta_{molar} = 100 * \theta_{obs/m} * d$$

where m is molar enzyme concentration (M) and d is the path length of the cell (cm). Spectra data was plotted as the mean with sample standard deviation in Prism 7.0a (GraphPad Software, Inc., La Jolla, CA) (Kelly et al., 2005). Sample standard deviation was calculated as described above.

For pH screen spectra, each sample contained 20 μM of enzyme prepared in different buffers: 10 mM citric acid pH 3, 10 mM sodium malonate pH 5, and 10 mM Tris pH 8. Scans were performed in a 1 mm path length cell from 300 to 190 nm with a data pitch of 0.5 nm and a 1 nm bandwidth. The scanning speed with 50 nm/minute and the temperature was held constant at 50°C Spectra were collected before incubation at 50°C (Time 0) and after 1 hour of incubation at 50°C (Time 60 minutes). The spectra for each buffer was subtracted from the corresponding sample spectra and raw ellipticity values were converted to molar ellipticity using equation (1). Spectra for each enzyme and pH were collected in duplicate.

QUANTIFICATION AND STATISTICAL ANALYSIS

Assays were performed in experimental duplicate or triplicate and this information is described in the corresponding figure legends. Assay data is presented as the mean of the experimental replicates +/− standard deviation of the sample. Sample standard deviation(s) was calculated using the equation:

$$s = \sqrt{\sum_{i=1}^{N} (x_i - \overline{x})^2} \Big/ (N - 1)$$

where N = is the number of observations in the sample, x_i are observed data points, and $\overline{x}$ is the sample mean.

DATA AND SOFTWARE AVAILABILITY

The nucleotide and amino acid sequence for the synthetic construct VP2.0 can be accessed at the NCBI GenBank (Accession No. MG252476).

URL: https://www.ncbi.nlm.nih.gov/genbank/